JOURNAL OF GEOPHYSICAL RESEARCH, VOL. 115, A05207, doi:10.1029/2009JA014751, 2010

Transient changes in magnetospheric-ionospheric currents caused by the passage of an interplanetary shock: Northward interplanetary magnetic field case

A. A. Samsonov,[1] D. G. Sibeck,[2] and Yiqun Yu[3]

Received 10 August 2009; revised 26 November 2009; accepted 9 December 2009; published 14 May 2010.

[1] We use results from a global MHD simulation to study the interaction of an interplanetary shock with the Earth's magnetosphere for a northward interplanetary magnetic field orientation. We connect intensifications of the transient northward Bz (NBZ) and Region 1 currents in the ionosphere with the appearance of two strong dynamo regions in the magnetosphere: the first on the high-latitude magnetopause near and behind the cusps and the second near the equatorial plane on the flanks. The ionospheric and magnetospheric transients are well synchronized and move antisunward gradually. According to the results obtained, the source of energy for the transient NBZ current is related to shock-intensified lobe reconnection, while the transient Region 1 current corresponds to the reflected fast shock predicted by Samsonov et al. (2007). We speculate that the electric circuits for the quasi-stationary field-aligned currents are similar to the transient electric circuits obtained in this paper.

Citation: Samsonov, A. A., D. G. Sibeck, and Y. Yu (2010), Transient changes in magnetospheric-ionospheric currents caused by the passage of an interplanetary shock: Northward interplanetary magnetic field case, *J. Geophys. Res.*, *115*, A05207, doi:10.1029/2009JA014751.

1. Introduction

[2] Systematic magnetic observations beginning in the nineteenth century revealed the simultaneous global changes of the magnetic field now known as geomagnetic sudden commencement (see review of *Araki* [1994, and references therein]). In the twentieth century, this phenomenon was explained in terms of solar wind discontinuities (interplanetary shocks and tangential discontinuities) impacting on the magnetosphere. *Araki* [1994] systematically studied ground magnetometer observations and drew a qualitative model for sudden commencements (SC). The disturbance magnetic field of the SC, D_{SC}, can be broken down into two parts [*Araki*, 1977, 1994]:

$$D_{SC} = DL + DP \tag{1}$$

where *DL* represents a step-function-like increase of the H component dominant near the equatorial plane and *DP* represents a two pulse structure dominant at high latitudes. The *DP* variation can be further broken down into two parts corresponding to the preliminary impulse (PI) with a duration about 1 min and the subsequent main impulse (MI)

$$DP = DP_{pi} + DP_{mi}. \tag{2}$$

[3] Using networks of magnetic observatories, equivalent current systems for the *DL*, DP_{mi} [*Obayashi and Jacobs*, 1957] and DP_{pi} [*Nagata and Abe*, 1955] were obtained. The equivalent current pattern for the *DL* is expressed as an axially symmetric (latitude-dependent) distribution around the pole that corresponds to a global magnetospheric compression caused by a solar wind dynamic pressure increase. The two-pulse structure of *DP* can be described by two pairs of equivalent current vortices at auroral latitudes, corresponding to the PI and MI. The current system responsible for the PI is a clockwise (counterclockwise) Hall current vortex in the postnoon (prenoon) sector. Opposite vortices are responsible for the MI: a counterclockwise (clockwise) current vortex in the postnoon (prenoon) sector. The ionospheric Hall currents are connected to field-aligned currents (FAC) as follows: the FAC flows downward (upward) in the postnoon (prenoon) sector during the PI and in the opposite directions during the MI.

[4] *Tamao* [1964a, 1964b] proposed a mechanism of the current system generation responsible for the PI. According to Tamao, the Alfvén (or more precisely the pure and converted transverse hydromagnetic) waves are generated in response to local increases in the magnetopause current as the interplanetary shock (IS) passes. The polarization charge at both edges of the enhanced current region creates a

[1]Department of Earth Physics, Saint Petersburg State University, Saint Petersburg, Russia.
[2]NASA Goddard Space Flight Center, Greenbelt, Maryland, USA.
[3]Department of Atmospheric, Oceanic and Space Science, University of Michigan, Ann Arbor, Michigan, USA.

0148-0227/10/2009JA014751

specific distribution of the electric potential (in agreement with that observed for the PI) which is transmitted to the ionosphere along magnetic field lines. *Tamao* [1964b] noted that the source of the transverse waves and of the corresponding FAC can also be the fast shock propagating through the magnetosphere. Therefore the electric current systems connecting either the dayside magnetopause or the fast shock with the ionosphere were assumed to appear in the transient stage after the IS passage.

[5] *Tamao* [1964b] explained the electric currents responsible for the MI in terms of azimuthal viscous stresses applied by the solar wind stream to the outer magnetospheric boundary. According to *Araki*'s [1994, Figure 12] qualitative model, the FAC during the MI is generated by a duskward electric field connected with enhanced magnetospheric convection in the compressed magnetosphere. However the above mentioned qualitative models do not specify the position of the magnetospheric dynamo for either current system. Recent global MHD simulations help draw a more detailed picture.

[6] The ideas of Tamao and Araki have been developed by *Fujita et al.* [2003a, 2003b] and *Kataoka et al.* [2004], who show numerical results obtained from Tanaka's global MHD model [*Tanaka*, 1994, 1995]. *Fujita et al.* [2003a, 2003b] explain the generation of the FAC associated with the PI and MI, respectively. In both papers, solar wind density increases from 10 cm^{-3} to 25 cm^{-3} with a constant northward interplanetary magnetic field (IMF) and a solar wind speed of 350 km/s. The FAC responsible for the PI is generated in the first two minutes after the solar wind discontinuity touches the nose of the magnetopause.They found that the FAC is connected to the dawn-to-dusk current flowing along the magnetopause (the Chapman-Ferraro current) via a radial current along the compression wave front in the outer magnetosphere and a dusk-to-dawn current in the inner magnetosphere. The FAC is converted from the cross-field current in magnetospheric regions of steep Alfvén velocity gradient in agreement with Tamao's initial assumption [*Tamao*, 1964b]. The magnetospheric dynamo (i.e., the region where $\mathbf{J} \cdot \mathbf{E} < 0$) in this current system is located at the dayside magnetopause.

[7] *Fujita et al.* [2003b] analyzed the evolution of magnetospheric plasma flows in the equatorial plane and defined two stages constituting the MI phase. In the first stage, the generator of the FAC system is supposed to be immediately behind the compression wavefront. The plasma first accelerates in the wavefront and then decelerates behind the wavefront providing the electromagnetic energy for the FAC generation. The FAC in the first stage flows downward on the dusk side and upward on the dawn side, i.e., has the same orientation as the FAC during the PI. *Fujita et al.* [2003b] noted that the FAC system in the second MI stage is similar to the known region 1 current [*Iijima and Potemra*, 1976] obtained previously in a quasi-stationary numerical MHD solution by *Tanaka* [1995]. The magnetospheric dynamo in this stage is supposed to be on the tailward side of the cusp. However the intensification of this dynamo (found to be a decrease of $\mathbf{J} \cdot \mathbf{E}$) occurs 2–3 minutes before the intensification of the corresponding FAC in the ionosphere. Therefore *Fujita et al.* [2003b] concluded that the generation of the current system in the equatorial region associated with the compression of the magnetospheric flanks may also contribute to the evolution of the FAC during the MI second stage.

[8] The interaction of a single density pulse with the magnetosphere was also simulated by *Keller et al.* [2002] using the BATS-R-US global MHD code. The solar wind density increases from 2.5 to 10 cm^{-3} for a constant solar wind velocity and a weak northward IMF. The BATS-R-US code predicts both Region 1 and northward Bz (NBZ) FACs in the initial quasi-stationary phase. When the compression wave propagates through the magnetosphere, a new current system having the same direction on the dawn and dusk flanks as the NBZ FAC forms rapidly. It intensifies a few minutes after the moment when the density pulse touches the magnetopause. Later this FAC moves antisunward and a new FAC system directed similar to the Region 1 current appears at lower latitudes. The latter current system evolves moving more slowly than the former one, but also extends into the antisunward direction. *Keller et al.* [2002] connected the first FAC with the pressure perturbation found in the equatorial plane near the magnetospheric boundary. The second FAC is supposed to be explained by the mode conversion of the fast compression wave following the initial ideas of Tamao. The dynamics of the simulated electric currents from *Keller et al.* [2002] generally agree with those found by *Moretto et al.* [2000] from ground-based magnetometer data for a sudden impulse event with similar solar wind conditions.

[9] Using the same numerical code as *Keller et al.* [2002], *Ridley et al.* [2006] simulated the magnetospheric and ionospheric response to an extremely strong IS. They obtain an evolution of the NBZ and Region 1 currents similar to that reported by *Keller et al.* [2002]. However they connect the source of the FAC intensification to the inward and outward magnetopause motion.

[10] The transient FACs connected with SC evolve gradually into a new steady FAC system [*Fujita et al.*, 2005]. This new state is similar to the initial state before the SC if the IMF orientation does not vary significantly during the event. Below we briefly review our knowledge about the quasi-stationary configuration of the magnetospheric-ionospheric currents for a steady northward IMF.

[11] *Dungey* [1963] postulated that northward IMFs reconnect with the geomagnetic field on the tail magnetopause behind the cusps. *Maezawa* [1976] studied polar cap convection using ground-based data both for northward and southward IMFs. Sunward convection over the polar cap occurs for IMF Bz >1 nT, while antisunward convection occurs for southward IMF. Detailed studies for northward IMF conditions [*Burke et al.*, 1979; *Rezhenov*, 1981] reveal a four cell convection pattern in agreement with the NBZ and Region 1 FACs. The NBZ FAC was carefully described by *Iijima et al.* [1984] using low-altitude spacecraft observation during intervals with Bz $\geq$ 5 nT. *Iijima et al.* [1984] noted that the NBZ current system intensifies and is more stable as the IMF Bz becomes more northward. The Region 1 and 2 FACs also exist for pure northward IMF intervals, but their intensity is lower than the intensity of the NBZ FAC.

[12] It can be difficult to visualize the global configuration of the magnetospheric-ionospheric currents, because extended regions in the magnetosphere map to relatively small ionospheric footprints. Variable IMF conditions result in

Table 1. Jumps of the MHD Parameters Through an Artificial Forward Fast Shock

	n_{sw}, cm^{-3}	Vx_{sw}, km/s	T_{sw}, 10^5 K	Bx_{sw}, nT	Bz_{sw}, nT
Upstream	5.0	−400	2.40	−1.71	4.70
Downstream	13.7	−527	8.98	−1.71	13.04

constantly changing FACs. Several authors [e.g., *Sonnerup*, 1980; *Troshichev*, 1982; *Stern*, 1983; *Siscoe et al.*, 1991] generalized the observed facts to draw a qualitative picture of the electric current configuration. Beginning from the middle of the 1990s, results from global MHD models with magnetospheric-ionospheric coupling gave a more quantitative description of the current systems.

[13] *Tanaka* [1995] reproduced the NBZ, Region 1 and 2 FACs in an MHD simulation for the northward IMF case and found that "on the evening side, the calculated region 1 currents flow almost along the field lines away from the Earth toward the magnetospheric low-latitude boundary layer (LLBL), then flow up the magnetopause across the field lines to high latitudes" (p. 12,057). The NBZ current is connected with currents in the distant low-latitude magnetotail. The magnetospheric dynamo for the Region 1 current is placed in the LLBL on both magnetospheric flanks, whereas "in the NBZ current loop, there is no remarkable driver or load" (p. 12,057). In further simulations, *Tanaka* [1999] connected ionospheric convection over the polar cap with the magnetospheric convection through the tail lobe stimulated by the cusp reconnection. Then *Tanaka* [2000, p. 58] concluded that "the anti-sunward momentum of the solar wind flow and its loading onto the open field lines through reconnection are the primary cause of the Region 1 FAC." Using the ISM global code, *Siscoe et al.* [2000] found several quasi-stationary solutions for different IMF orientations and obtained current systems similar to those of *Tanaka* [1995] for the northward IMF case.

[14] Our review shows that MHD codes have simulated both a stationary configuration and transient variations in the magnetosphere-ionosphere currents. However the drivers of the intensive FACs caused by the IS passage were generally assumed to be explained in terms of different mechanisms than the drivers of the stable stationary FACs obtained for constant solar wind conditions. In this work, we intend to show that the transient and stationary FACs are more similar than previously thought and that the energy drivers may have common sources.

2. Numerical Model and Boundary Conditions

[15] The interaction of an IS with the magnetosphere has been simulated by the global BATS-R-US code [*Powell et al.*, 1999]. The BATS-R-US code solves the MHD equations with a finite volume discretization in a 3-D block-adaptive Cartesian grid using conservative variables. The supersonic solar wind conditions are imposed on a plane perpendicular to the Sun-Earth line (X axis) upstream from the bow shock. There is an outflow boundary at $X = -255\ R_E$. The inner numerical boundary is located about 3 R_E from the Earth. The boundary conditions fix the mass density and allow no mass flux and no gradient of the thermal pressure through this boundary. The magnetic field near the inner boundary is determined primarily by the imposed terrestrial magnetic field [*Gombosi et al.*, 2003]. Near this boundary, the field-aligned current is calculated by $(\nabla \times \mathbf{B}) \cdot \mathbf{b}$ (where $\mathbf{B}$ is magnetospheric magnetic field, and $\mathbf{b}$ is the unit vector of $\mathbf{B}$) and mapped down to the ionosphere using relation $J_i/J_m = B_i/B_m$ (where indices m and i stand for magnetosphere and ionosphere, respectively). Based on this FAC source and height-integrated conductivity pattern in the ionosphere, the electric potential is solved in the ionospheric electrodynamic model. The potential is then mapped back to the magnetospheric boundary, where the electric field and corresponding plasma drift velocity $\mathbf{V} = (\mathbf{E} \times \mathbf{B})/B^2$ are calculated, providing the inner boundary velocity condition (see *Ridley et al.* [2004] for more details). Since the boundary allows no mass flux to flow through, the radial component of the drift velocity is then removed. In this simulation run, the height-integrated Pedersen and Hall ionospheric conductivities are uniform and equal to 5 mho. No corotation velocity is applied at the inner boundary. The magnetic dipole axis is forced to align along the rotation axis.

[16] An increased grid resolution has been requested, the region with the smallest computational cell $0.125 \times 0.125 \times 0.125\ R_E^3$ extends from the subsolar magnetopause toward the low and high-latitude magnetopause flanks nearly to $X = -10\ R_E$.

[17] Table 1 summarizes values of the MHD parameters upstream and downstream from the artificial IS. The simulated IS is similar to the one studied previously by *Samsonov et al.* [2007]. Both shocks have similar density and velocity jumps; the IMF points northward (with $By = 0$), but *Samsonov et al.* [2007] took the angle θ_{BV} between the IMF and the solar wind velocity (coincident with the X axis) upstream of the IS equal to 45 degrees, while now we take it equal to 70 degrees. As usual, the shock normal points along the X axis. From the Rankine-Hugoniot conditions, we obtain a shock fast Mach number $M_f = V_{sh}/V_f = 7.96$ (where shock velocity V_{sh} = 600 km/s and $V_f = \sqrt{C_s^2 + V_A^2}$ = 75.4 km/s, C_s and V_A are the sound and Alfvén velocities, respectively).

[18] The model was run for two hours for constant preshock solar wind conditions. The IS entered the sunward boundary with a rise time of 10 s. We continued the simulation with the constant postshock conditions until a new quasi-stationary state was obtained in the magnetosphere.

3. Results From the Simulation

[19] The IS is launched from the sunward boundary at $x = 33\ R_E$ and reaches the subsolar magnetopause ($x \simeq 11\ R_E$) nearly four minutes later. We fix the latter moment as a reference time t = :00:00 (:mm:ss) and study the subsequent transient processes in the magnetosphere and ionosphere.

[20] Figures 1 and 2 illustrate the evolution of the electric current and convection velocity in the ionosphere. The color-coded portions show the magnitude of the radial current density J_R, while arrows show the direction and magnitude of the velocity every 15 s beginning from t = :01:00. Since the IS only touches the subsolar point at t = :00:00, the disturbance in the ionosphere appears only one minute later. The length of the arrows is proportional to the velocity magnitude, but is normalized to the maximum

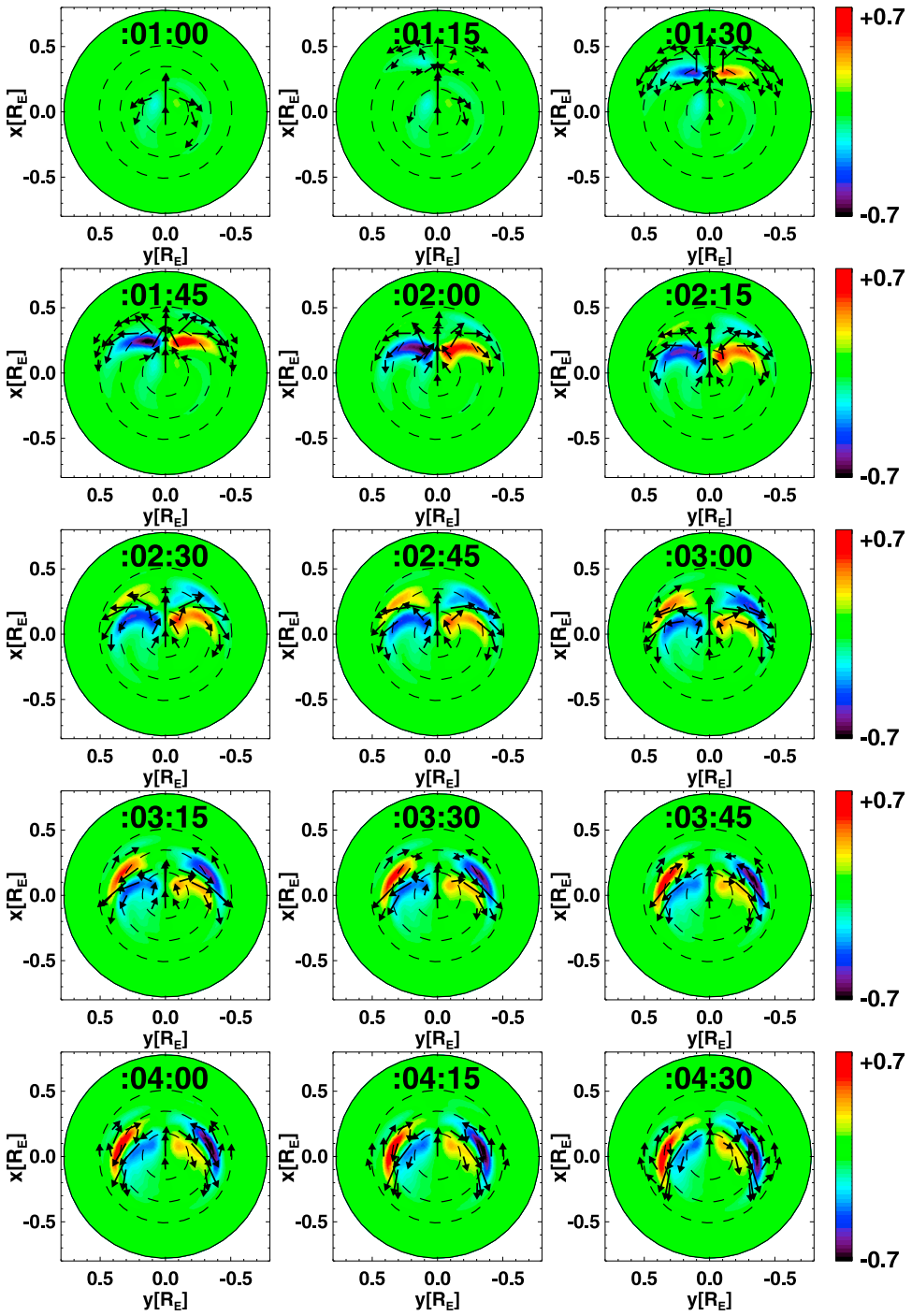

Figure 1. Variations in the northern ionosphere caused by the IS passage. Color bars indicate the magnitude of the radial current density in $\mu A/m^2$, and arrows illustrate the direction and magnitude of the velocity. Only high velocities are shown by arrows (see details in text). Noon is above; midnight is below. Each plot shows the time in :mm:ss format.

velocity V_{max} at each time and only arrows with $|V| > 0.3\ V_{max}$ are shown.

[21] The parameters J_R and V in the first panel correspond to the initial quasi-stationary state before the SC (here the SC means a FAC disturbance caused by the IS). The magnitude of both J_R and V at this time is only 20–25% of maximum enhanced J_R and V in the very disturbed state at t = :02:00 (only 1 minute later). Global MHD codes successfully predict two large-scale FACs: the Region 1 and NBZ currents. Both current systems (although very weak) are shown in the first panel; the NBZ current is at latitude $\theta > 80°$, and the Region 1 current in interval $70° < \theta < 80°$. A negative J_R indicates a downward FAC, while a positive J_R indicates an upward FAC. There is sunward convection near

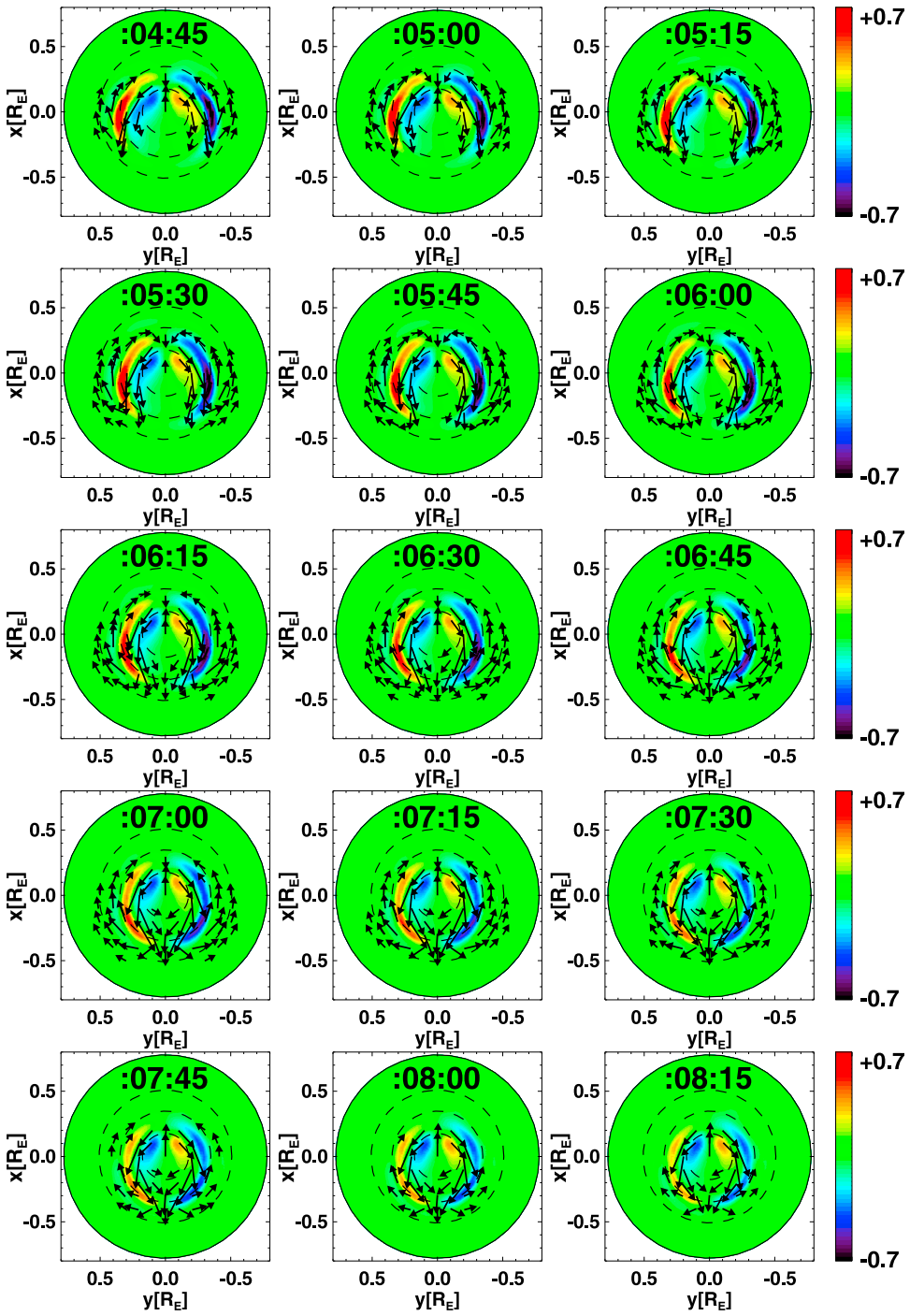

Figure 2. The same parameters as in Figure 1 at later times.

the noon-midnight meridian and a return antisunward flow between the NBZ and R1 FACs. This convection pattern agrees with expectations for magnetopause reconnection behind the cusp.

[22] Beginning from the second panel, a new FAC pair appears somewhere close to the dayside cusp (at $\theta \sim 70°$ near the noon meridian). This current system intensifies greatly in a half minute and moves first poleward and then along polar (70°–80°) latitudes antisunward. The direction of the FAC coincides with the direction of the NBZ current. Moreover, following the evolution in Figure 2 we conclude that the new FAC really becomes a steady NBZ current in the postshock quasi-stationary state. The two velocity vortices of the FAC (on the dusk and dawn sides) gradually evolve to become the velocity vortices of the NBZ current. We call this current system the "transient NBZ FAC."

[23] The transient NBZ FAC reaches its maximum strength ($J_R \simeq 0.77\ \mu A/m^2$) at $t \simeq$:02:00. Nearly at the same time, another current system becomes visible near the noon meridian at somewhat lower latitudes for θ between 60° and

70°. Because this FAC flows in the direction of the R1 current therefore we call it the "transient R1 FAC." The transient R1 FAC intensifies and moves poleward and antisunward slower than the transient NBZ FAC. It reaches maximum strengths $J_R \geq 0.8\ \mu A/m^2$ between :04:00 and :06:00 at which time it is located near $\theta \sim 70°$, straddling the terminator plane $X = 0$. Later, the transient R1 FAC continues to move antisunward nearly along the same latitude, but after :07:00 both the morning and evening currents split into two parts. One part of each current moves toward the midnight meridian and gradually diminishes in strength, while another part having maximum values in the midmorning or in the late afternoon forms a new steady R1 FAC. The transient R1 FAC results in two velocity vortices with antisunward flow at higher latitudes (where they overlap with the vortices of the transient NBZ FAC) and sunward flow at lower latitudes.

[24] Figures 1 and 2 show that the intensifications of both FACs occur in relatively short time intervals and the maximum value of the transient NBZ current is observed 2–4 minutes before the maximum R1 FAC. The source of the energy for both FACs lies in the magnetosphere and can be found by inspecting $\mathbf{E} \cdot \mathbf{J}$ values. If $(\mathbf{E} \cdot \mathbf{J}) < 0$, the plasma kinetic energy is transformed into electromagnetic energy which intensifies the FACs. We assume a good correspondence in time between large negative $\mathbf{E} \cdot \mathbf{J}$ values in the magnetosphere and FAC intensifications since the propagation time for the Alfvén wave from the magnetosphere to the ionosphere usually does not exceed 1 minute. Figure 3 shows the magnitude of $\mathbf{E} \cdot \mathbf{J}$ in the magnetosphere with the same 15 s time resolution beginning from $t =$:01:00. We draw contours in the $Z = 0$ plane (Figure 3, top) and in the $Y = 0$ plane (Figure 3, bottom).

[25] Recall that the bow shock and the magnetic barrier in front of the magnetopause are dynamo regions $(\mathbf{E} \cdot \mathbf{J}) < 0$ because the magnetic field magnitude increases along the flow lines there. The IS is a load $(\mathbf{E} \cdot \mathbf{J}) > 0$ because the plasma accelerates at the shock front. Magnetic reconnection regions are loads because they transform electromagnetic energy into kinetic. However, motion of the reconnected field lines may result in an accumulation of the magnetic field in another region nearby where a new dynamo appears.

[26] In the first panel of Figure 3, the fast shock, labeled "FS," lies in the X interval from +5 to +6 R_E in the equatorial magnetosphere and magnetosheath. Two blue regions sunward of the IS front are the magnetic barrier (nearly coinciding with the magnetopause for the northward IMF case) and the bow shock. The FS in the subsolar magnetosphere reaches the inner numerical boundary at $X \simeq 3\ R_E$ in the next 15 s and then reflects from the boundary and propagates sunward (for references to previous studies of reflected FS, see section 4). At $t =$:01:30 in the equatorial plane, a new dynamo region becomes visible in the subsolar magnetosphere at a distance of ~6 R_E from the Earth (as indicated by the red arrow). Since the reflected (or reverse) fast shock decelerates the plasma flow, we conclude that this new dynamo region is connected with the reflected shock. In the next several frames, the dynamo region in the outer magnetosphere convects with the plasma flow toward the flanks (while the subsolar part moves through the magnetosheath to the bow shock). The former dynamo is accompanied by a velocity vortex marked by antisunward flow farther from the Earth and sunward flow closer to the Earth.

[27] Now consider what happens during the first two minutes in the noon-meridional plane (Figure 3, bottom). The FS increases the magnetosheath magnetic field strength and compresses the magnetosphere and therefore intensifies magnetic reconnection behind the cusp. The site of the magnetic reconnection region is marked "REC" in Figure 3. The region with accelerated plasma near the magnetopause corresponds to $(\mathbf{E} \cdot \mathbf{J}) > 0$, but reconfiguration of the magnetic field results in a dynamo region nearby, on the magnetospheric side of the reconnection region. We will discuss the mechanism for this dynamo in section 4.

[28] The consecutive plots for the noon-meridional plane illustrate first a rapid intensification of both the reconnection load and the nearby dynamo (from :01:30 to :02:00 or :02:30) and then a smooth relaxation. Although reconnection still occurs in the last plots in Figure 3, it becomes almost invisible because of the fixed color scale.

[29] According to these results, there are only two well determined regions of the magnetospheric dynamo, one of them in the equatorial plane and the other one in the noon-meridional plane. However, these two planes may not reflect a complete picture. Therefore we present twelve cuts through the magnetosphere in planes parallel to the XY plane (Figure 4, top) and twelve cuts parallel to the XZ plane (Figure 4, bottom). This lets us show the three-dimensional shape of the dynamo regions outside the two restricted planes. At the fixed time ($t =$:03:00) shown in Figure 4, both the equatorial and high-latitude dynamos are well defined. The two symmetric equatorial dynamos occur at Y about $\pm 8\ R_E$ near the terminator plane and become substantially weaker above the equatorial plane at $Z = 3 - 4\ R_E$. The two high-latitude dynamos (behind the north and south cusps) are more extended in both the Y and Z directions. Comparing with Figure 3, we note that the high-latitude dynamo is still very strong, while the equatorial dynamo is just beginning to intensify. The dynamo regions can approach each other as shown, for example, in the $Y = 8\ R_E$ plane.

[30] The two ionospheric currents and the two magnetospheric dynamos maximize in a specific order during short time intervals, and these times only slightly overlap. This gives us the possibility of establishing a direct correspondence between the FACs and the dynamo regions, using their time synchronization. Figure 5 shows plots for the ionosphere and the magnetospheric equatorial and noon-meridional planes at four particular times. The first moment $t =$:01:45 corresponds to the rapid intensification of the transient NBZ FAC and a strong dynamo appears at the same time around the cusp. This magnetospheric disturbance occurs almost immediately after the passage of the shock, which itself approaches the terminator plane at this moment.

[31] At the next two times, $t =$:02:45 and $t =$:03:45, the NBZ FAC decreases while the R1 FAC intensifies. A corresponding evolution occurs in the magnetosphere: the dynamo region near the high-latitude magnetopause becomes weaker, and the dynamo in the flank equatorial magnetosphere grows substantially. At the final time :04:45, the NBZ FAC is less than it was previously, and the high-latitude dynamo is also weaker. In contrast, both the R1 FAC and

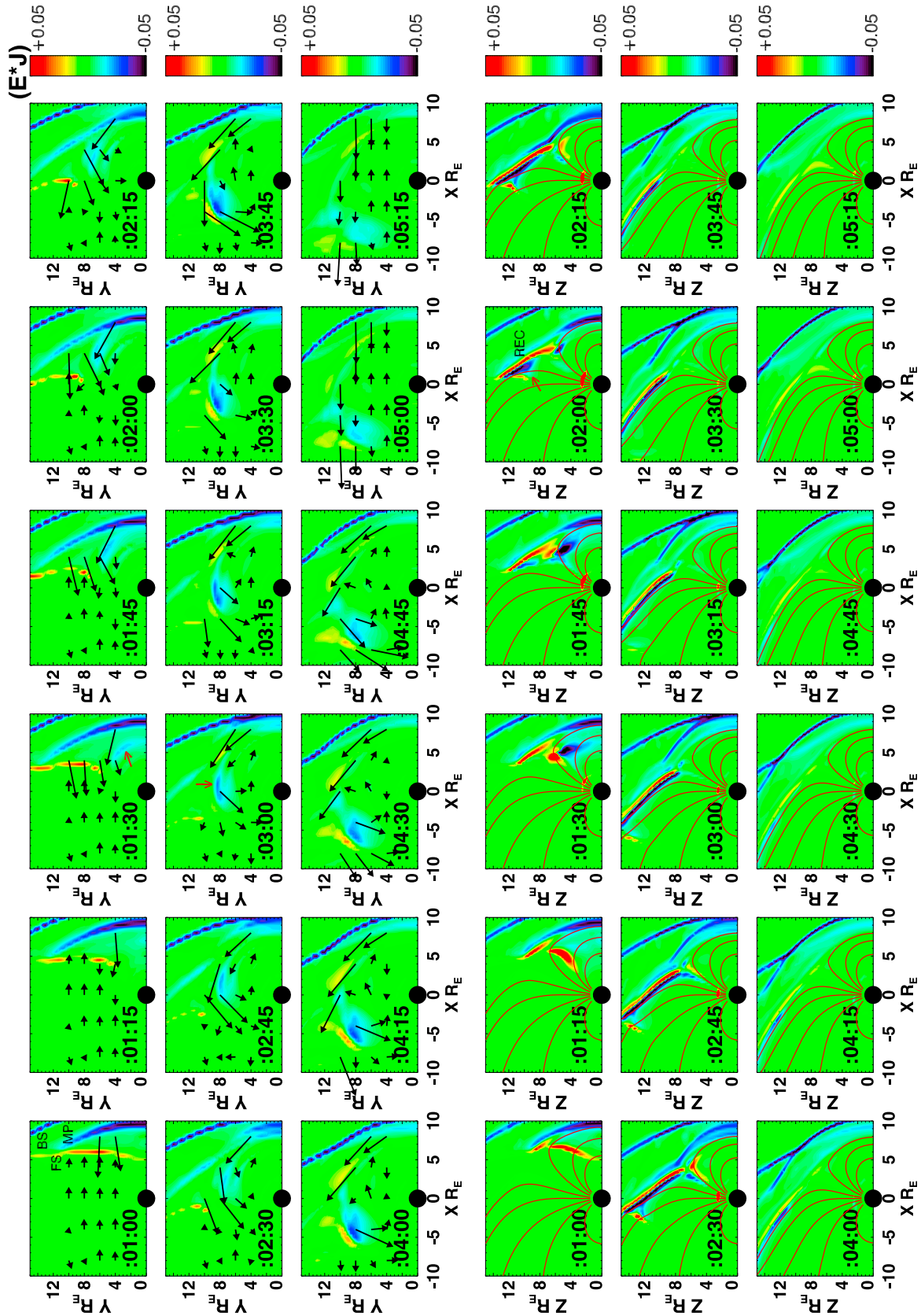

Figure 3. The magnitude of $\mathbf{E} \cdot \mathbf{J}$ in nW/m^3 in the (top) $Z = 0$ and (bottom) $Y = 0$ planes. Arrows in Figure 3 (top) show velocity; red lines in Figure 3 (bottom) indicate closed field lines. The abbreviations "FS," "MP," and "BS" refer to the forward fast shock, magnetopause, and bow shock, respectively. "REC" marks the reconnection site behind the cusp. Red arrows point to the magnetospheric dynamo regions.

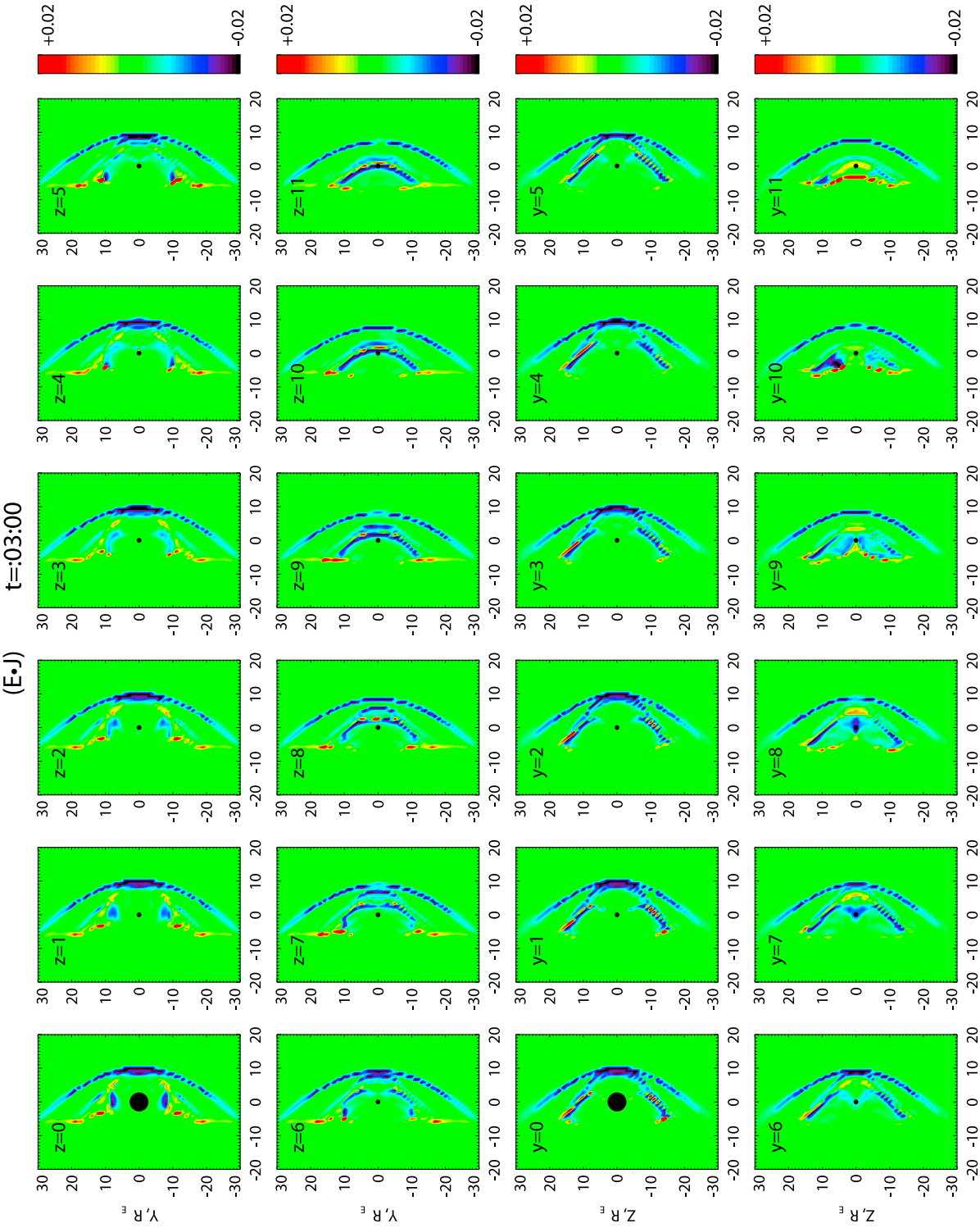

Figure 4. The magnitude of $\mathbf{E} \cdot \mathbf{J}$ in nW/m^3 at a fixed time :03:00 in a series of planes parallel to the equatorial or noon-meridional plane (as shown by the Y and Z values in R_E).

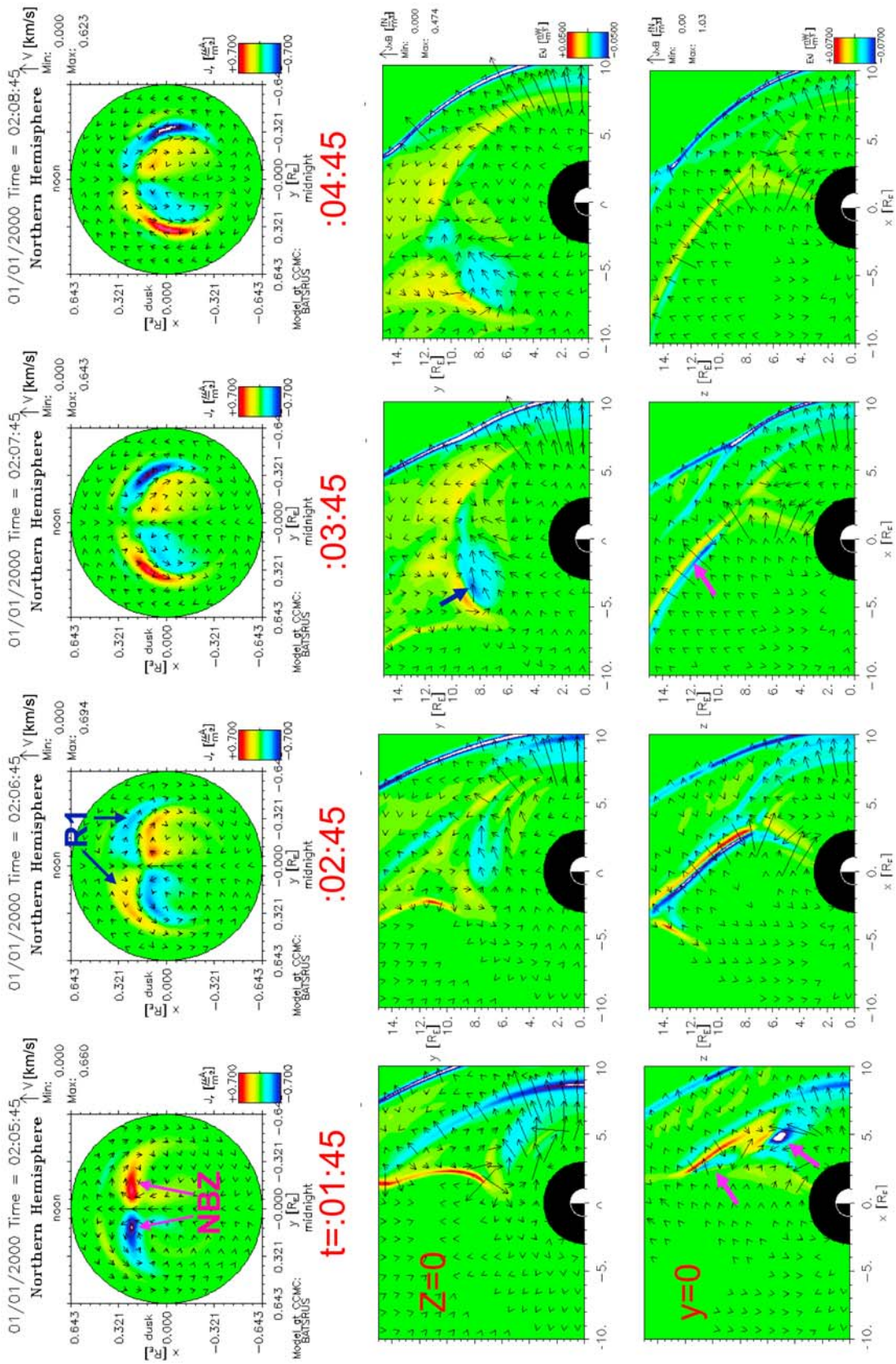

Figure 5. Illustration of radial ionospheric currents and $\mathbf{E} \cdot \mathbf{J}$ in the magnetosphere at four selected times (as indicated). Arrows in the ionospheric plots show the velocity, while arrows in the magnetospheric plots show $\mathbf{J} \times \mathbf{B}$. Purple arrows indicate the NBZ FAC current and corresponding dynamos, while blue arrows indicate the Region 1 FAC and its dynamo. White color in the strong dynamo regions means that $\mathbf{E} \cdot \mathbf{J}$ is below the given color range.

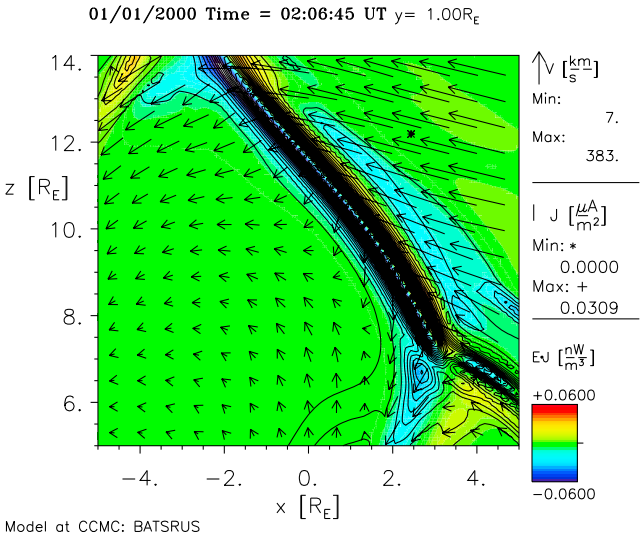

Figure 6. Parameters $\mathbf{E} \cdot \mathbf{J}$ (colors) and $\mathbf{J}$ (contours) at $t =$:02:45 in a selected region (with $Y = 1\ R_E$) near the high-latitude magnetopause where the magnetic reconnection is assumed to occur for the northward IMF case. The arrows show the direction and magnitude of the flow velocity.

the equatorial dynamo at :04:45 are nearly as strong as at :03:45.

[32] Figure 5 shows a clear antisunward displacement of the FACs and the dynamos. This is an indication of transient processes caused by the FS passage through the magnetosphere and magnetosheath. The velocity at which the magnetospheric dynamo regions propagate is close to the shock velocity in the magnetosphere. After :08:00 both the ionospheric currents (Figure 2) and the magnetospheric variations diminish, and a new quasi-stationary configuration appears.

4. Discussion

[33] We need to discuss the source of energy for the magnetospheric dynamo regions found in section 3. At the beginning, let us show the meaning of negative $\mathbf{E} \cdot \mathbf{J}$ using the ideal MHD assumption:

$$(\mathbf{E} \cdot \mathbf{J}) = -((\mathbf{V} \times \mathbf{B}) \cdot \mathbf{J}) = ((\mathbf{J} \times \mathbf{B}) \cdot \mathbf{V}) < 0 \qquad (3)$$

When Ampère's force $\mathbf{J} \times \mathbf{B}$ is directed opposite to the flow velocity, the plasma decelerates, and the plasma kinetic energy is transformed into magnetic energy (and partly into thermal energy as at the bow shock). The magnetic energy accumulated in the magnetosphere can later be released in the ionosphere via FACs. Arrows in Figures 5 (middle) and 5 (bottom) show the direction of Ampère's force. This force is really directed against the velocity (the flow velocity in the equatorial and noon-meridional planes is shown in Figures 3 and 6, respectively).

[34] As is known from dayside magnetospheric physics, magnetic reconnection for southward IMF conditions permits solar wind plasma entry into the magnetosphere in the subsolar region. By contrast, plasma enters through the high-latitude magnetopause for strongly northward IMF orientations. Figure 6 shows a X-Z cut at $Y = 1\ R_E$ near the high-latitude magnetopause behind and near the cusp at $t =$:02:45 when the corresponding dynamo is still rather strong. There is a plasma flow (shown by arrows) through the magnetopause in this region. The current layer (shown by contours) includes both the load and dynamo regions which are both aligned with the magnetopause. A small part of the FS is shown in the top left corner, and the cusp is in the bottom right corner.

[35] The equatorial dynamo is obviously not related to magnetic reconnection. In our previous study [*Samsonov et al.*, 2007], using the same global MHD code, we have shown that the FS reflects from the inner numerical boundary of the simulation box, and a reflected shock (or fast wave) moves sunward through the outer magnetosphere and magnetosheath resulting in outward magnetopause and bow shock motion [see also *Samsonov et al.*, 2006; *Cable et al.*, 2007; *Šafránková et al.*, 2007]. As discussed by *Samsonov et al.* [2007], this artificial numerical boundary in reality may correspond to the ionosphere or some other physical boundary within the inner magnetosphere. The reflected (or reverse) FS decelerates the plasma flow and increases the magnetic field magnitude and density. This is consistent with energy transformation in a dynamo region. The temporal evolution of the equatorial dynamo shown in Figure 3 (and discussed above) confirms its connection to the reflected FS.

[36] We do not present the global configuration of the transient magnetospheric-ionospheric currents after the IS passage in this paper. An often used method is to draw electric current streamlines directly from the numerical results. However we find the accuracy of this method low. One first needs to find the curl of the magnetic field vector and then to trace streamlines of the current vector. This problem becomes more complicated near the Earth where the dipole field is much stronger than the field of external sources, and a small numerical error related to grid interpolation may result in significant deviations in the current lines.

[37] Meanwhile, some remarks about the electric current configuration can be made without any simulation. The high-latitude radial currents in Figures 1 and 2 are almost equivalent to the field-aligned currents (positive J_R corresponds to negative $J_\parallel$ in the north hemisphere). It is generally known that the polar cap is magnetically connected with high-latitude regions in the outer magnetosphere and magnetotail, for example, the plasma mantle [*Vasyliunas*, 1979]. The ionospheric footprints from the dayside auroral oval seem to be connected to the low-latitude boundary layer. This configuration generally agrees with the connections between the NBZ and R1 FACs, from one side, and the high-latitude and equatorial dynamo regions, from the other side, presented in this paper. Note that the transient NBZ current obtained in the simulation forms in the dayside polar cap and the transient R1 FAC near the auroral oval.

[38] As Figure 2 shows, the transient FACs gradually evolve into a new quasi-stationary current system corresponding to constant solar wind parameters after the IS. Therefore we assume that the stationary magnetospheric-ionospheric current system may be configured similar to the transient one. The NBZ FAC is again connected with the magnetopause region behind the cusp adjacent to the re-

connection site. The source of energy for the R1 FAC may arise from the quasi-viscous interaction in the low-latitude boundary layer as was predicted by *Sonnerup* [1980].

[39] We do not discuss in this paper the conversion of fast mode waves into transverse waves as described by *Tamao* [1964a] and implicitly assumed by subsequent authors. MHD simulations have never directly confirmed this conversion. Instead, we conclude that another mechanism explains the generation of the transient FACs and do not invoke mode conversion.

[40] Because we employed a version of the BATS-R-US code that does not couple to the Rice Convection model or other inner magnetosphere models, we have not simulated Region 2 FACs. However the Region 2 current is supposed to be connected with the partial ring current, and we believe that this current system does not change in the first minutes of the interaction before the shock front passes the magnetotail.

5. Conclusions

[41] This paper presents results from a global MHD simulation with the BATS-R-US code of the interaction between an IS and the Earth's magnetosphere. We investigate transient variations of the field-aligned currents in the ionosphere and connect them to the evolution of the magnetospheric dynamo regions. In the ionosphere, the transient NBZ FAC increases to its maximum value about 2 min (t = :02:00) after the time when the IS just touches the subsolar bow shock. The maximum transient R1 FAC occurs between :04:00 and :06:00. This sequence of FAC intensifications agrees with the well-known PI-MI sequence in magnetic observations.

[42] Two dynamo regions inside the magnetosphere are found: one is near the high-latitude magnetopause behind the cusp adjacent to the typical reconnection site for the northward IMF conditions, the other one is in the outer magnetosphere near the equatorial plane. The first dynamo peaks about two minutes earlier than the second one. Using the good synchronization between the ionospheric and magnetospheric variations, we conclude that the high-latitude dynamo provides energy for the NBZ FAC, while the equatorial dynamo powers the R1 FAC. The postulated magnetic field connection between the ionospheric and magnetospheric regions is consistent with expectations [*Vasyliunas*, 1979].

[43] The ionospheric FACs and magnetospheric dynamos evolve, changing their intensity and moving mainly in the antisunward direction. However, the transient NBZ FAC changes its position only slightly and stays mostly in the dayside region during the whole time interval, while the transient R1 FAC extends and moves from the vicinity of subsolar point to the nightside region and finally splits into two parts. One of the parts staying in the dayside ionosphere forms a new steady R1 FAC, while the other part moves toward midnight and gradually disappears. This behavior agrees with the evolution of the magnetospheric dynamo regions. The high-latitude dynamo initially appears just around the cusp and then extends and moves antisunward along the magnetopause. It also includes extended regions on the morning and evening sides. But its ionospheric footprint hardly moves after the first two minutes. On the contrary, the equatorial dynamo corresponding to the R1 FAC propagates from the dayside magnetosphere through the dawn and dusk magnetospheric flanks toward the plasma sheet. This dynamo is accompanied by a velocity vortex, and the direction of the magnetospheric convection in the vortex corresponds to the direction of the ionospheric convection around the R1 FAC. Figure 3 shows the equatorial dynamo split in two near :04:00. One of the parts then convects into the plasma sheet, while the other part forms a new steady dynamo region located possibly in the low-latitude boundary layer.

[44] The transient ionospheric FACs resulting from the IS passage gradually evolve into a quasi-stationary configuration corresponding to the postshock solar wind conditions. This is the main reason for us to believe that the quasi-stationary magnetospheric-ionospheric current system is generally similar to the transient one. Again the dynamo of the NBZ current is related to magnetic field redistribution near the reconnection site behind the cusps, while the Region 1 dynamo can obtain its energy from the quasi-viscous interaction in the low-latitude boundary layer [*Sonnerup*, 1980].

[45] The predictions made in this paper can be verified observationally. In particular, we predict an intensification in the lobe reconnection rate immediately after a shock passage, which can be checked using either spacecraft (e.g., by Cluster) or ground observations. We already know [*Boudouridis et al.*, 2007] that the solar wind dynamic pressure pulses intensify dayside magnetopause reconnection rates for southward IMF orientation.

[46] We have also shown that the predicted equatorial dynamo region is related to velocity and magnetic field vortices on the flanks. Similar vortices have been observed by spacecraft and seen in MHD simulations [e.g., *Collado-Vega et al.*, 2007]. They were explained in terms of the Kelvin-Helmholtz instability. However we predict them to be transient phenomena lasting only several minutes after the shock passage.

[47] The transient ionospheric variations obtained in this paper using an MHD simulation of the interaction between the IS and the magnetosphere mainly agree with results from previous studies. However, our interpretation of the results based on a direct correspondence of ionospheric currents and magnetospheric dynamos differs from other interpretations which usually follow the mode conversion explanation by *Tamao* [1964a]. According to *Wilson and Sugiura* [1961] and *Tamao* [1964a], the azimuthal drag force in the outer magnetosphere produces magnetic field vortices whose sense of rotation agrees with that required for the direction of the R1 FAC. Since the azimuthal drag is stronger near the equatorial plane, this explanation may be consistent with the predicted equatorial dynamo regions in our study (although our explanation is different). Meanwhile, the connection of the transient NBZ FAC with the intensification of high-latitude magnetopause reconnection after the shock passage for northward IMF conditions has not been noted or discussed in previous works.

[48] **Acknowledgments.** The work was supported in part by NASA's THEMIS project and in part by grant of Russian President NSH-1243.2008.5 and GK grant N 02.740.11.0331. Simulation results

have been provided by the Community Coordinated Modeling Center (CCMC) at Goddard Space Flight Center through their public Runs on Request system (http://ccmc.gsfc.nasa.gov). In particular, we have studied the run "Andrey_Samsonov_120507_1." The BATS-R-US Model was developed by the CSEM group at the University on Michigan. The authors thank the reviewers for valuable comments.

[49] Wolfgang Baumjohann thanks Athanasios Boudouridis, Joachim Vogt, and another reviewer for their assistance in evaluating this paper.

References

Araki, T. (1977), Global structure of geomagnetic sudden commencements, *Planet. Space Sci.*, *25*, 373–384.

Araki, T. (1994), A physical model of the geomagnetic sudden commencement, in *Solar Wind Sources of Magnetospheric Ultra-Low-Frequency Waves*, *Geophys. Monogr. Ser.*, vol. 81, edited by M. J. Engebretson, K. Takahashi, and M. Scholer, pp. 183–200, AGU, Washington, D. C.

Boudouridis, A., L. R. Lyons, E. Zesta, and J. M. Ruohoniemi (2007), Dayside reconnection enhancement resulting from a solar wind dynamic pressure increase, *J. Geophys. Res.*, *112*, A06201, doi:10.1029/2006JA012141.

Burke, W. J., M. C. Kelley, R. C. Sagalyn, M. Smiddy, and S. T. Lai (1979), Polar cap electric field structures with a northward interplanetary magnetic field, *Geophys. Res. Lett.*, *6*, 21–24.

Cable, S., Y. Lin, and J. L. Holloway (2007), Intermediate MHD shocks with a terrestrial magnetopause, *J. Geophys. Res.*, *112*, A09202, doi:10.1029/2007JA012419.

Collado-Vega, Y. M., R. L. Kessel, X. Shao, and R. A. Boller (2007), MHD flow visualization of magnetopause boundary region vortices observed during high-speed streams, *J. Geophys. Res.*, *112*, A06213, doi:10.1029/2006JA012104.

Dungey, J. W. (1963), The structure of the exosphere or adventures in velocity space, in *Geophysics, The Earth's Environment*, edited by C. DeWitt, J. Hieblot, and A. Lebeau, pp. 503–550, Gordon and Breach, New York.

Fujita, S., T. Tanaka, T. Kikuchi, K. Fujimoto, K. Hosokawa, and M. Itonaga (2003a), A numerical simulation of the geomagnetic sudden commencement: 1. Generation of the field-aligned current associated with the preliminary impulse, *J. Geophys. Res.*, *108*(A12), 1416, doi:10.1029/2002JA009407.

Fujita, S., T. Tanaka, T. Kikuchi, K. Fujimoto, and M. Itonaga (2003b), A numerical simulation of the geomagnetic sudden commencement: 2. Plasma processes in the main impulse, *J. Geophys. Res.*, *108*(A12), 1417, doi:10.1029/2002JA009763.

Fujita, S., T. Tanaka, and T. Motoba (2005), A numerical simulation of the geomagnetic sudden commencement: 3. A sudden commencement in the magnetosphere-ionosphere compound system, *J. Geophys. Res.*, *110*, A11203, doi:10.1029/2005JA011055.

Gombosi, T. I., et al. (2003), Adaptive mesh refinement for global magnetohydrodynamic simulation, in *Space Plasma Simulation*, *Lecture Notes Phys.*, vol. 615, edited by J. Büchner, C. Dum, and M. Scholer, pp. 247–274, Springer, Berlin.

Iijima, T., and T. A. Potemra (1976), The amplitude distribution of field-aligned currents at northern high latitudes observed by Triad, *J. Geophys. Res.*, *81*, 2165–2174.

Iijima, T., T. A. Potemra, L. J. Zanetti, and P. F. Bythrow (1984), Large-scale Birkeland currents in the dayside polar region during strongly northward IMF: A new Birkeland current system, *J. Geophys. Res.*, *89*, 7441–7452.

Kataoka, R., H. Fukunishi, S. Fujita, T. Tanaka, and M. Itonaga (2004), Transient response of the Earth's magnetosphere to a localized density pulse in the solar wind: Simulation of traveling convection vortices, *J. Geophys. Res.*, *109*, A03204, doi:10.1029/2003JA010287.

Keller, K. A., M. Hesse, M. Kuznetsova, L. Rastätter, T. Moretto, T. I. Gombosi, and D. L. DeZeeuw (2002), Global MHD modeling of the impact of a solar wind pressure change, *J. Geophys. Res.*, *107*(A7), 1126, doi:10.1029/2001JA000060.

Maezawa, K. (1976), Magnetospheric convection induced by the positive and negative Z components of the interplanetary magnetic field: Quantitative analysis using polar cap magnetic records, *J. Geophys. Res.*, *81*(13), 2289–2303.

Moretto, T., A. J. Ridley, M. J. Engebretson, and O. Rasmussen (2000), High-latitude ionospheric response to a sudden impulse event during northward IMF conditions, *J. Geophys. Res.*, *105*, 2521–2532, doi:10.1029/1999JA900475.

Nagata, T., and S. Abe (1955), Notes on the distribution of SC* in high latitudes, *Rep. Ionos. Res. Jpn.*, *9*, 33–44.

Obayashi, T., and J. A. Jacobs (1957), Sudden commencements of magnetic storms and atmospheric dynamo action, *J. Geophys. Res.*, *62*, 589–616.

Powell, K. G., P. L. Roe, T. J. Linde, T. I. Gombosi, and D. L. de Zeeuw (1999), A solution-adaptive upwind scheme for ideal magnetohydrodynamics, *J. Comput. Phys.*, *154*, 284–309.

Rezhenov, B. (1981), Convection at high latitudes when the interplanetary magnetic field is northward, *Planet. Space Sci.*, *29*, 687–693.

Ridley, A., T. Gombosi, and D. Dezeeuw, (2004), Ionospheric control of the magnetosphere: Conductance, *Ann. Geophys.*, *22*, 567–584.

Ridley, A. J., D. L. de Zeeuw, W. B. Manchester, and K. C. Hansen (2006), The magnetospheric and ionospheric response to a very strong interplanetary shock and coronal mass ejection, *Adv. Space Res.*, *38*, 263–272, doi:10.1016/j.asr.2006.06.010.

Šafránková, J., Z. Němeček, L. Přech, A. A. Samsonov, A. Koval, and K. Andréeová (2007), Modification of interplanetary shocks near the bow shock and through the magnetosheath, *J. Geophys. Res.*, *112*, A08212, doi:10.1029/2007JA012503.

Samsonov, A. A., Z. Němeček, and J. Šafránková (2006), Numerical MHD modeling of propagation of interplanetary shock through the magnetosheath, *J. Geophys. Res.*, *111*, A08210, doi:10.1029/2005JA011537.

Samsonov, A. A., D. G. Sibeck, and J. Imber (2007), MHD simulation for the interaction of an interplanetary shock with the Earth's magnetosphere, *J. Geophys. Res.*, *112*, A12220, doi:10.1029/2007JA012627.

Siscoe, G. L., W. Lotko, and B. U. O. Sonnerup (1991), A high-latitude, low-latitude boundary layer model of the convection current system, *J. Geophys. Res.*, *96*, 3487–3495.

Siscoe, G. L., N. U. Crooker, G. M. Erickson, B. U. Ö. Sonnerup, K. D. Siebert, D. R. Weimer, W. W. White, and N. C. Maynard (2000), Global geometry of magnetospheric currents inferred from MHD simulations, in *Magnetospheric Current Systems*, *Geophys. Monogr. Ser.*, vol. 118, pp. 41–52, AGU, Washington, D. C.

Sonnerup, B. U. O. (1980), Theory of the low-latitude boundary layer, *J. Geophys. Res.*, *85*, 2017–2026.

Stern, D. P. (1983), The origins of Birkeland currents, *Rev. Geophys.*, *21*, 125–138.

Tamao, T. (1964a), The structure of three-dimensional hydromagnetic waves in a uniform cold plasma, *J. Geomagn. Geoelectr.*, *16*, 89–114.

Tamao, T. (1964b), A hydromagnetic interpretation of geomagnetic SSC*, *Rep. Ionos. Space Res. Jpn.*, *18*, 16–31.

Tanaka, T. (1994), Finite volume TVD scheme on an unstructured grid system for three-dimensional MHD simulation of inhomogeneous systems including strong background potential fields, *J. Comput. Phys.*, *111*, 381–390.

Tanaka, T. (1995), Generation mechanisms for magnetosphere-ionosphere current systems deduced from a three-dimensional MHD simulation of the solar wind-magnetosphere-ionosphere coupling processes, *J. Geophys. Res.*, *100*, 12,057–12,074.

Tanaka, T. (1999), Configuration of the magnetosphere-ionosphere convection system under northward IMF conditions with nonzero IMF B_y, *J. Geophys. Res.*, *104*, 14,683–14,690.

Tanaka, T. (2000), Field-aligned-current systems in the numerically simulated magnetosphere, in *Magnetospheric Current Systems*, *Geophys. Monogr. Ser.*, vol. 118, pp. 53–59, AGU, Washington, D. C.

Troshichev, O. A. (1982), Polar magnetic disturbances and field-aligned currents, *Space Sci. Rev.*, *32*, 275–360.

Vasyliunas, V. M. (1979), Interaction between the magnetospheric boundary layers and the ionosphere, in *Magnetospheric Boundary Layers*, edited by J. Lemaire, *Eur. Space Agecy Spec. Publ., ESA SP-148*, 387–393.

Wilson, C. R., and M. Sugiura (1961), Hydromagnetic interpretation of sudden commencements of magnetic storms, *J. Geophys. Res.*, *66*, 4097–4111.

A. A. Samsonov, Department of Earth Physics, Physical Faculty, Saint Petersburg State University, Saint Petersburg, 198504, Russia. (samsonov@geo.phys.spbu.ru)

D. G. Sibeck, NASA Goddard Space Flight Center, Greenbelt, MD 20771, USA.

Y. Yu, Department of Atmospheric, Oceanic and Space Science, University of Michigan, Ann Arbor, MI 48109, USA.